


## Article

# Verification of the EURO-CORDEX RCM Historical Run Results over the Pannonian Basin for the Summer Season

Irida Lazić \*, Milica Tošić and Vladimir Djurdjević \* 

Faculty of Physics Institute for Meteorology, University of Belgrade, Dobračina 16, 11000 Belgrade, Serbia; milica.tosic@ff.bg.ac.rs

\* Correspondence: irida.lazic@ff.bg.ac.rs (I.L.); vdj@ff.bg.ac.rs (V.D.)

**Abstract:** In previous projects that focused on dynamical downscaling over Europe, e.g., PRUDENCE and ENSEMBLES, many regional climate models (RCMs) tended to overestimate summer air temperature and underestimate precipitation in this season in Southern and Southeastern Europe, leading to the so-called summer drying problem. This bias pattern occurred not only in the RCM results but also in the global climate model (GCM) results, so knowledge of the model uncertainties and their cascade is crucial for understanding and interpreting future climate. Our intention with this study was to examine whether a warm-and-dry bias is also present in the state-of-the-art EURO-CORDEX multi-model ensemble results in the summer season over the Pannonian Basin. Verification of EURO-CORDEX RCMs was carried out by using the E-OBS gridded dataset of daily mean, minimum, and maximum near-surface air temperature and total precipitation amount with a horizontal resolution of 0.1 degrees (approximately 12 km × 12 km) over the 1971–2000 time period. The model skill for selected period was expressed in terms of four verification scores: bias, centered root mean square error (RMSE), spatial correlation coefficient, and standard deviation. The main findings led us to conclude that most of the RCMs that overestimate temperature also underestimate precipitation. For some models, the positive temperature and negative precipitation bias were more emphasized, which led us to conclude that the problem was still present in most of the analyzed simulations.

**Keywords:** EURO-CORDEX; summer drying problem; regional climate model evaluation; E-OBS; Pannonian Basin; temperature; precipitation



**Citation:** Lazić, I.; Tošić, M.; Djurdjević, V. Verification of the EURO-CORDEX RCM Historical Run Results over the Pannonian Basin for the Summer Season. *Atmosphere* **2021**, *12*, 714. <https://doi.org/10.3390/atmos12060714>

Academic Editor: Alexandre M. Ramos

Received: 30 April 2021  
Accepted: 28 May 2021  
Published: 31 May 2021

**Publisher's Note:** MDPI stays neutral with regard to jurisdictional claims in published maps and institutional affiliations.



**Copyright:** © 2021 by the authors. Licensee MDPI, Basel, Switzerland. This article is an open access article distributed under the terms and conditions of the Creative Commons Attribution (CC BY) license (<https://creativecommons.org/licenses/by/4.0/>).

## 1. Introduction

To carry out more realistic regional climate simulations, climate models demand the representation of processes from global and large scales to regional and local scales. Hence, climate-change impacts on communities require tools, such as regional climate models (RCMs), to complement the results of global climate models (GCMs) [1]. Consequently, the output of RCMs is primarily used as initial information for assessments on possible climate change in the future and its potential future risks to socioeconomic or environmental sectors. However, during the last three decades of regional climate modeling research and development, RCMs have evolved into multipurpose modeling tools [2].

Dynamic downscaling represents a method of using the RCM at a finer resolution to improve the results of coarse-scale GCMs. RCMs are driven by GCM lateral boundary conditions (LBCs), and they modulate the driver's results at local scales due to the higher spatial resolution and the more complex physics described in the models [3–5]. GCMs capture complex topographical mountainous regions exceedingly smoothed due to coarse spatial resolution [6]. Hence, RCMs add regional detail as a response to regional-scale forcing, such as topography, with more explicitly described physics in the model as a result of increasing spatial resolution (e.g., References [4,7]).

This issue of “added value” using RCMs has been demonstrated in many studies, especially for simulation of precipitation over areas with complex topography, such as the Alpine region, which are well known to affect precipitation [7,8] with the emphasized enhanced effect during summer convective rainfall [9,10]. Even in the absence of topography, due to a better representation of underlying physics parameterizations, RCMs generate more credible climate change signals with the observed climatological data [7,11–13]. Although RCMs are anticipated to add the value of downscaling at scales that are not resolved by the GCMs, they can also improve results on the large scales of the driving GCM [14].

For decades, the climate research community has put efforts toward achieving a large ensemble to cover all uncertainty sources in future climate projections at regional to local scales [15]. Through international science coordination and partnerships, successive CMIP (Coupled Model Intercomparison Project) initiatives were established by WCRP (The World Climate Research Programme) to study and intercompare GCMs to provide large ensembles [16,17]. On the other hand, European projects such as PRUDENCE, ENSEMBLES, and EURO-CORDEX (the European branch of the international CORDEX initiative) put efforts to achieve high-resolution climate descriptions based on RCMs. The RCM community has grown rapidly during the CORDEX (Coordinated Regional Climate Downscaling Experiment) project as the main reference framework for regional dynamical downscaling research [2]. For instance, EURO-CORDEX is derived from the accomplishments of former EU projects such as PRUDENCE and ENSEMBLES [18]. The EURO-CORDEX projection ensemble has a high-resolution (0.11 degrees), which has not been attained in previous projects, that offers a more robust assessment of climate change projections over Europe and defines the degree of uncertainty indicating alternative developments [2,17–19]. The benefits of using RCM ensembles are particularly evident if the focus is on localized extreme weather events due to the demand for high-resolution probabilistic climate change information [2,19], which is crucial for risk-based impact studies.

Despite the fact that RCMs have constantly improved over decades, some prominent scientific issues remain, so the scientific community needs to consider these issues. One of the remaining issues known to the larger scientific community is the so-called “summer drying” problem attributed to RCM climate simulations over certain parts of Europe. According to [20] and former studies [21], dry and warm biases during the summer over southeastern Europe are mainly attributed to RCMs, although they are less visible in GCM results. The main reason for too dry and too warm climate simulation is mainly not related to systematic errors in the large-scale general circulation. As shown in Reference [20], the reduction in the summer drying problem could be a result of improving the physical parameterization and land-surface parameter distribution constructed by Reference [22] in RCMs, as well as improving the dynamics in RCMs [21,23].

Seneviratne et al. [24] examined the influence of soil moisture coupling in RCMs. Soil moisture plays an important role in the climate system as a source of water for the atmosphere. Soil moisture is related to evapotranspiration from land, a major component of the continental water cycle and significant energy flux. Consequently, soil moisture–climate interactions and feedbacks are manifested through impacts on temperature and precipitation [25]. According to the impact of soil moisture on evapotranspiration variability, three soil moisture regimes are important to climate models: dry, transitional, and wet. Regimes vary in space and are sensitive to the soil, climate, and vegetation characteristics [26]. The transitional regime associated with the strongest impact of soil moisture on evapotranspiration and large mean evapotranspiration is important due to uncertainties in RCMs related to soil moisture–atmosphere coupling [24,27]. From spring to summer, in central Europe and parts of the Mediterranean, the soil moisture regime shifts from wet soils to a transitional regime [26]. As a consequence, soil moisture–atmosphere coupling can strongly affect temperature variability in regions such as the Mediterranean for the present climate and Central and Eastern Europe for the future climate [24]. Anders et al. [28] took a step toward decreasing dry and warm biases during summer in a small part of Southeast Europe by changing soil characteristics, although these model biases still remain in this

region. Hence, as shown in previous studies, the “summer drying” problem still represents a field of examination, and to better understand the sources and reasons for the summer drying problem, further research is needed.

RCMs driven by quasi-observed boundary conditions (ERAs) that have participated in the MERCURE project (Modeling European Regional Climate: Understanding and Reducing Errors) showed warm and dry bias during summer, which represents typical RCM features in a large drainage basin known as the Danube catchment [23,29]. The Pannonian Basin can be considered a subdomain of the Danube catchment. With an almost enclosed structure, the Pannonian Basin represents an outstanding natural laboratory for studying the physical processes of interest [30]. The Pannonian basin is very interesting from the geographical point of view, but also it is one of the most intensive agriculture production areas in Europe, so it is of great importance to understand future climate impacts, and before that step, understanding the quality of available RCM results, is a starting point. In recent decades, enriched regions with rich plant and food production have been affected by more frequent extreme events, such as heatwaves, droughts, and extreme precipitation [31–34]. According to climate projections, the Pannonian Basin appears to be more vulnerable in the future and among the hotspot regions with the highest impacts on socioeconomic sectors [30,33]. Hence, the overall aim of the present study is to investigate the credibility of RCMs in EURO-CORDEX multi-model ensembles to simulate surface air temperature and precipitation in the Pannonian Basin due to the well-known “summer drying” problem [35–38]. Because RCMs are driven by GCMs, simulation biases are a combination of both GCM and RCM biases originating from a variety of sources [38,39], so uncertainty in RCMs is described as a ‘cascade of uncertainty’ [40]. To provide a beneficial basis for policy-making, uncertainty in RCM simulations must be accounted for as much as possible. The data and study area, observation gridded E-OBS dataset, evaluated RCM simulations, applied methods, and evaluation metrics are discussed in Section 2. Section 3 presents the analysis of EURO-CORDEX RCM performance to simulate the mean, maximum, and minimum temperatures and precipitation over the Pannonian Basin. Section 4 provides the main conclusions and a summary of this study.

## 2. Materials and Methods

### 2.1. Data and Study Area

To verify EURO-CORDEX RCMs over the Pannonian Basin, daily model results were extracted from the EURO-CORDEX database [18,19] and compared with data derived from the E-OBS gridded dataset [41]. The following datasets with a horizontal resolution of 0.11 degrees (approximately 12 km × 12 km) were used for comparison: daily mean near-surface air temperature, minimum near-surface air temperature, maximum near-surface air temperature, and precipitation (hereafter referred to as *tas*, *tasmin*, *tasmax*, and *pre*, respectively).

The verification area shown in Figure 1 is the subdomain in the center of the region bounded by longitudes, 14° E and 27° E, and latitudes, 43.5° N and 50° N, in which topographic elevation is below 200 m. According to the fact that the Pannonian valley is a large lowland area surrounded by mountains, we focused in this study on verification statistics calculation exclusively over the valley part of the wider region, specifically the part which is under certain terrain altitude. Our decision was driven by the fact that this area was known for the temperature and precipitation biases presented in the previous publications, which clearly coincided with the lowland terrain. In many other papers, model verification is mainly focused and calculated over regular rectangular geographical areas, which means that in our case and with our approach, the area-averaged errors can be hidden by mixing results over lowland and surrounding mountains. With our approach, we tried to extract as much as possible information about these biases focusing on a very specific area (not regular), both in terms of topography, but also in terms of the model error position. This subdomain is introduced to remove the impact of scores acquired over surrounding mountains on the average score value for the Pannonian Valley.

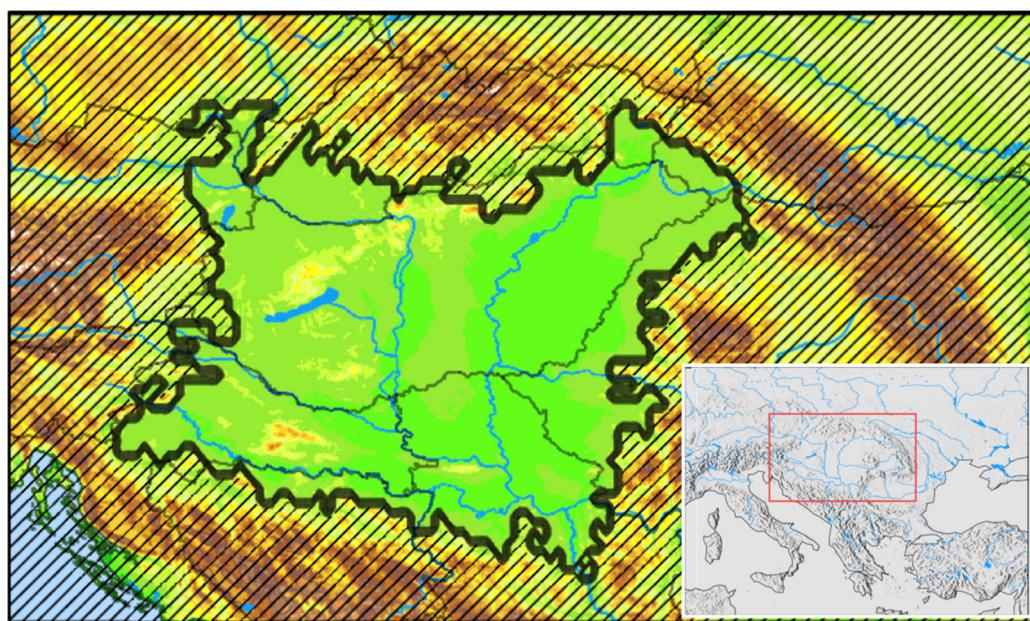


**Figure 1.** The Pannonian Basin, central valley is indicated as a not-hatched area that is also bounded by the thick black line. In the bottom right corner, the wider Southeast Europe region is given with the red rectangle indicating boundaries of the main figure.

The Pannonian Basin, also known as the Carpathian Basin or Central Danubian Basin, is one of the world's largest enclosed basins and lies in the southeastern part of central Europe. The basin is surrounded by the Alps in the northwest, the Carpathian Mountains in the northeastern, and the Dinaric Alps in the southwest direction and represents a subdomain of the Danube catchment. The basin is centered on the territory of Hungary, northern Serbia, northeast Croatia, northeastern Slovenia, eastern Austria, western Slovakia, western Ukraine, and western Romania. During the Miocene and Pliocene epochs, a shallow ancient Pannonian Sea existed in this region, so the Pannonian Basin is a valuable natural laboratory for the study of the water and energy cycles [30,36]. Additionally, the orographic characteristics of the relatively flat and homogeneous central part of the basin with an excellent observational network allow us to study some processes in detail, such as land–surface interactions, precipitation systems, surface energy, and water budgets. [36]. In accordance with these facts, the main goal of the Pannonian Basin Experiment, which is a part of the Global Energy and Water Exchanges (GEWEX) project of the WCRP, is to better understand Earth system components and their interactions in the Pannonian Basin.

#### 2.1.1. Observation Gridded Data

The E-OBS dataset arranged by the ECA&D initiative and derived through interpolation of European Climate Assessment and Data (ECA&D) station data [41–43] covers the period back to 1950 over Europe and provides the mean across a generated 100-member ensemble of each daily field, which represents a “best-guess” field [41,42]. The E-OBS database consists of daily interpolations of temperature (maximum, mean, and minimum daily values), precipitation, and mean sea-level pressure and provides gridded fields at a horizontal resolution of  $0.1^\circ$  in regular latitude/longitude coordinates. The standard error is presented through estimation of uncertainty of the best-guess value and calculated as the difference between the 5th and 95th percentiles over the ensemble. The density of stations used for the interpolations varies over time and domain, although errors in precipitation are more severe than those in temperature [44]. The insufficient spatial density of stations in the E-OBS data is one of the main sources of uncertainty with an emphasized effect on precipitation [44–46]. The Pannonian Basin is a region that has a smaller density of stations than parts of western and central Europe and the United Kingdom [41]; thus, a further

increase in observation density is expected [36]. However, the E-OBS dataset remains a crucial dataset for model validation [47,48] and climate monitoring across Europe. Moreover, uncertainties related to reference data should be considered when evaluating climate model output, especially for the precipitation field because it is more sensitive to selection reference data [49,50].

As the main representation of the observed climate, we used the state-of-the-art daily gridded dataset E-OBS with a horizontal resolution of  $0.11^\circ$ . In this study, we extracted and examined the daily mean near-surface air temperature, minimum near-surface air temperature, maximum near-surface air temperature, and precipitation.

### 2.1.2. EURO-CORDEX RCM Simulations

Nine RCMs driven by GCM from the EURO-CORDEX framework evaluated in this work are introduced in detail in the references mentioned in Table 1. Lateral boundary conditions (LBCs) were provided by GCMs from the Coupled Model Intercomparison Project Phase 5 (CMIP5). We considered all the RCMs that fulfilled the following requirements: daily averaged temperature (mean, minimum, and maximum) and daily averaged precipitation available at the highest resolution  $0.11^\circ$  for RCM simulations forced by GCM historical run. To be more precise, we analyzed all available high-resolution runs from the EURO-CORDEX database. We found this fact is important, for the reason that other published results that include model verification are mainly focused on the subset of available ensemble runs (not the largest possible one), often because the selected subset is used for some further investigation, e.g., different impact studies in agriculture, forestry, water resources, etc. In total, there were 30 available and evaluated RCM simulations for the 1971–2000 time period, with different combinations of RCMs and GCMs or with different realizations of the same GCM (marked in Table 1 in the third column with labels r1, r2, r12 or r3). The same RCM is driven by different GCMs to assess the effect of LBCs on downscaling realization. Different realizations of the same GCM, whereby the same GCM was initiated from different times within a long control integration, were introduced to estimate the impact of simulated natural variability on climate change responses [51]. Likewise, different versions of the same RCMs were used for validation (REMO2009 and REMO2015, ALADIN 5.3 and ALADIN 6.3). For the periods of 1951–1980 and 1961–1990, there were 23 available and evaluated simulations in the GCM–RCM simulation matrix; therefore, validation for these periods is available in the Supplementary Materials.

The EURO-CORDEX data used in this work can be found at the website <https://www.euro-cordex.net/060378/index.php.en> (accessed on 30 May 2021), by choosing a specific European node where data are distributed.

## 2.2. Methods

### 2.2.1. Extracting a Specific Region and Regridding

To prepare data for comparing GCM–RCM simulations with the E-OBS gridded dataset, we used the software “Climate Data Operators” (CDO) [52]. We selected a wider region bounded by longitudes,  $14^\circ$  E and  $27^\circ$  E, and latitudes,  $43.5^\circ$  N and  $50^\circ$  N. Then, since the RCMs and E-OBS datasets do not share the same horizontal grid, all RCM data were interpolated onto a common grid spacing of  $0.11^\circ$  related to the E-OBS grid. Regridding was performed by the bilinear interpolation method. To obtain evaluation metrics over the low elevation part of the Pannonian Basin, we made a mask in the selected region (Figure 1) consisting of a binary matrix (0,1) in which a value of 1 represents a grid point with topographic elevation below 200 m. To create a compact subdomain, few exceptions from elevation constraints were made. Afterward, the calculated evaluation metrics over a low elevation subregion were divided by using this binary matrix.

**Table 1.** Overview of RCMs used in the present study. Numbers in the last column are used to distinguish different RCM–GCM combinations in this paper (references for each RCM are given in Reference [19]).

Institution	RCM	Driving Model (s)	Integration Number
CNRM (Météo France)	ALADIN 5.3	CNRM-CM5 r1	1
CNRM (Météo France)	ALADIN 6.3	CNRM-CM5 r1	2
RMIB-UGent (Royal Meteorological Institute of Belgium and Ghent University)	ALARO-0	CNRM-CM5 r1	3
CLMcom (CLM Community with contributions by BTU, DWD, ETHZ, UCD, WEGC)	CCLM 4.8.17	CNRM-CM5 r1	4
		EC-EARTH r12	5
		HadGEM2-ES r1	6
		MPI-ESM-LR r1	7
		CNRM-CM5 r1	8
		EC-EARTH r12	9
		EC-EARTH r1	10
DMI (Danish Meteorological Institute, Copenhagen, Denmark)	HIRHAM 5	EC-EARTH r3	11
		HadGEM2-ES r1	12
		NCC-NorESM1-M r1	13
		CNRM-CM5 r1	14
		EC-EARTH r12	15
		EC-EARTH r1	16
		EC-EARTH r3	17
KNMI (Royal Netherlands Meteorological Institute, Ministry of Infrastructure and the Environment)	RACMO 2.2E	HadGEM2-ES r1	18
		CNRM-CM5 r1	19
		EC-EARTH r12	20
		EC-EARTH r3	21
		IPSL-CM5A-MR	22
		HadGEM2-ES r1	23
		MPI-ESM-LR r1	24
SMHI (Rosby Centre, Swedish Meteorological and Hydrological Institute, Norrköping Sweden)	RCA 4	NCC-NorESM1-M r1	25
		MPI-ESM-LR r1	26
		MPI-ESM-LR r2	27
		IPSL-CM5A-LR r1	28
		NCC-NorESM1-M r1	29
		NOAA-GFDL-GFDL	30
		ESM2G r1	
GERICS (Climate Service Center Germany, Hamburg, Germany)	REMO 2009		
GERICS (Climate Service Center Germany, Hamburg, Germany)	REMO 2015		

### 2.2.2. Evaluation Metrics

In this study, we focused on variables, such as temperature (mean, minimum, and maximum) and precipitation, to examine whether warm and dry biases existed during summer in the Pannonian Basin. Therefore, evaluation is conducted on the raw RCM output without bias adjustment for the 30-year reference period of 1971–2000. This study does not consider bias adjustment. The period of 1971–2000 is a high-quality meteorological dataset, so further investigation is based upon this reference period. For brevity, evaluations for the periods of 1951–1980 and 1961–1990 are given in the Supplementary Materials.

The degree of statistical similarity between two climatic fields was determined by using the Taylor diagram to provide a concise statistical summary. The diagram, which was first proposed by Taylor [53], captures different statistics of the observed and model seasonal fields, such as spatial standard deviation, centered RMSE, and spatial correlation. The output of each RCM model in comparison with E-OBS (performing as reference) can be shown on the same diagram thanks to the geometric relationship between these metrics. The radial distances between the origin to each symbol related to RCM outputs and E-OBS are proportional to the standard deviation. The centered RMS (root mean square) error in the simulated field is proportional to the distances along concentric circles of each symbol from the reference point hereafter depicted with a star symbol on the diagram. The Pearson spatial correlation coefficient between the RCM output and the reference is shown by the azimuthal location of a symbol in the Taylor diagram. As a result, the symbols for the best-performing RCMs are placed nearest to this reference point.

There is a distinct difference between the RMS difference and the centered RMS difference in the Taylor diagram, which is the bias-corrected RMSE. The centered RMS difference is analogous to the standard deviation of a typical model error, and in the model evaluation, the centered RMSE is a more common term in quantifying the correspondence between two patterns [53].

In addition to the statistical summary obtained by the Taylor diagram, the spatial distributions of temperatures and precipitation biases for each GCM–RCM analyzed combination, and the overall bias of the ensemble are averaged over the 1971–2000 period during summer to investigate the summer drying problem that occurred in the Pannonian Basin in detail. In some cases, for evaluation bias occurring in the precipitation field, biases are expressed as % of observations. Additionally, bias was averaged over the 1971–2000 period and the Pannonian Basin and presented in this work. Additionally, the ability of the models to reproduce the mean temperature trend was estimated during the 1970–2005 period.

### 3. Results and Discussion

The ability of models to simulate the current climate is crucial, as significant biases restrict our understanding of potential climate impacts, including extreme weather. In this work, we used EURO-CORDEX RCMs with a horizontal high grid resolution ( $0.11^\circ$ ), which is currently the best available horizontal resolution on the EURO-CORDEX framework. Therefore, we did not compare (in the sense of resolution and its effect of “added value”) different resolutions of RCM simulations. Previous studies have shown that in the Carpathian region, high-resolution RCM simulations ( $0.11^\circ$ ) were better than medium resolution ( $0.44^\circ$ ) in model evaluation compared with observation data, especially in the sense of representing the precipitation field during summer when the majority of convective processes occurs within the study area [37]. On the other hand, in Reference [37], the spread of RCM simulations with higher grid resolution did not decrease, which was likely a consequence of the pronounced internal surface variability on small scales due to orographic forcing and heterogeneous surfaces or because of the intensified biases that originate from LBCs in GCMs [54]. To summarize, high-resolution RCM simulations were more reliable in representing the frequency distribution of weather phenomena than minimizing biases [4,7].

The contribution of GCMs and RCMs to the biases is not examined in this work, but these biases originate from various sources. Furthermore, Vautard et al. [38] discovered that the GCM contribution to the overall bias is greater for mean and maximum daily temperature than the RCM itself in flat areas, and it is reversed for daily minimum temperature. This difference is explained by the fact that during the night, when the atmosphere is stratified and when the daily minimum temperature is observed, model biases are strongly dependent on stable boundary layer parameterizations and turbulence, low-level clouds, and the characteristics of the land surface, which are the main sources of uncertainty in the RCM [38]. This RCM’s contribution is larger in summer due to lighter winds, which evoke less mixing in the atmosphere [38]. Vautard et al. [38] showed that in most cases, the RCM contribution outweighs the GCM contribution for minimum temperatures, and it is systematically greater than for mean temperatures. On the other hand, maximum temperatures are expected to be determined by soil–atmosphere interactions [38]. Regarding the precipitation field, GCM and RCM have an equal contribution to the overall bias since both large-scale drivers, and local physical parameterizations play a role in defining biases [38]. Hence, according to these results, we evaluated the mean, maximum and minimum temperature and precipitation fields with respect to the E-OBS gridded dataset for the 1971–2000 period. RCMs’ performances for periods of 1951–1980 and 1961–1990 were not shown here for brevity due to similar performances, but they are shown in Supplementary Materials.

Before moving to the RCM data evaluation in terms of temperature and precipitation statistics, it is necessary to show the ability of RCMs to simulate climate characteristics, such as temperature and precipitation, during the year and over the region of interest. The annual cycles of monthly averaged mean temperature and monthly precipitation across the domain of the Pannonian Basin are depicted in Figure 2. The data in Figure 2 come from the E-OBS database, as well as the EURO-CORDEX RCM11 ensemble ( $0.11^\circ$  grid). Across the Pannonian Basin, the temperature maximum is observed in July and August, while the temperature minimum is observed in December and January. Summer (June and July) brings the most precipitation to the Pannonian Basin, while winter (January and February) brings the least precipitation. The annual temperature cycle is mostly reproduced by the RCM ensemble median, with small departures from the E-OBS dataset with values up to  $1^\circ\text{C}$ . The RCM ensemble median underestimates temperature in winter (December, January, February) and spring (March, April, and May), while overestimation is observed in summer (June, July, and August). In autumn (September, October, November), the ensemble temperature median coincides with the E-OBS dataset with the smallest spread of RCM simulations (area between the 5th percentile and 95th percentile). On the other hand, the RCM ensemble median underestimates precipitation in summer, while overestimation is present in all other seasons during the year. Notably, RCMs have the largest spread of their simulations in late spring (May) and summer when most convective processes occur in the Pannonian Basin, which indicates RCM uncertainty in representing precipitation during this part of the year.

First, we investigated the ensemble overall temperature bias and precipitation bias. The 5th, median and 95th percentiles of temperature and precipitation biases among the 30 GCM-RCM simulations (cited in Table 1) for all four seasons are shown in Figure 3. These percentile maps indicate that not all models are biased in the same way, as we can see that the 5th percentile maps contain the most negative biases and the 95th percentile maps contain the most positive biases for temperature and precipitation biases. However, the exception is the winter season, where even the lower tail (5th percentile map) of the bias distribution is positive. This finding indicates that most RCMs tend to overestimate precipitation in winter (at least 95% of the RCMs have a positive bias).

According to the median of bias distribution, the most prominent feature in Figure 3 is mostly widespread warm and dry bias during summer. The temperature median ranges from  $-1.2$  to  $+1.6^\circ\text{C}$ , and the precipitation median ranges from  $-38\%$  to  $+33\%$ . The positive temperature and negative precipitation biases were even more pronounced for certain models, meaning the issue still exists in most examined simulations in the Pannonian Basin during the summer season. The upper tail of the temperature bias distribution (95th percentile map) is positive everywhere across the Pannonian Basin with biases up to  $4^\circ\text{C}$ . The lower tail of the temperature bias distribution (5th percentile map) is negative everywhere with values below  $-2^\circ\text{C}$  in some parts, which indicates that some models tend to underestimate temperature. For the maximum and minimum temperatures, the same reveals that overall ensemble biases appeared in summer (not shown for shortness). On the other hand, the upper tail of the precipitation bias distribution (95th percentile map) is mainly positive across the Pannonian Basin with biases up to  $+70\%$ . The lower tail of the precipitation bias distribution (5th percentile map) is negative everywhere, with values below  $-50\%$  in some parts of the Pannonian Basin. Consequently, in this study, the main goal is to further examine in detail the existing summer drying issue in the Pannonian Basin and to inspect each individual RCM from the EURO-CORDEX multi-model ensemble.



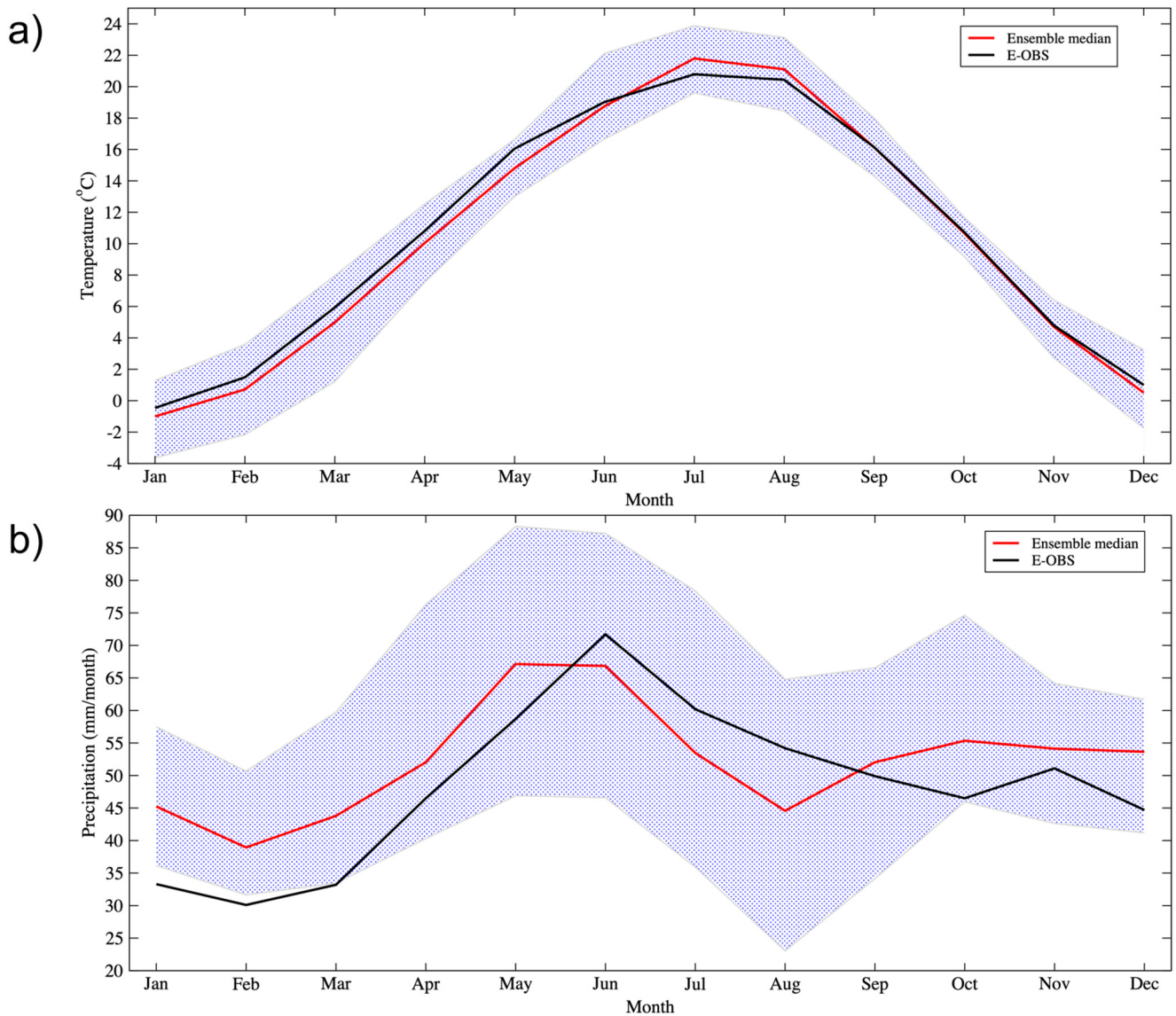


**Figure 2.** Monthly mean (a) temperature and (b) precipitation averaged over the Pannonian Basin for 1971–2000. The black line depicts the E-OBS dataset, the red line depicts the median of the RCM ensemble distribution, and the violet shaded region denotes the area between the 5th percentile and 95th percentile of the RCM distribution.

Figures 4 and 5 represent the spatial distribution of the mean (1971–2000) GCM–RCM bias for each individual model of the summer (June–July–August, or JJA) mean temperature field and precipitation field, respectively, with respect to the E-OBS gridded dataset. Principally, there is spatial correspondence between temperature and precipitation biases, which is mostly pronounced during the summer as warm and dry biases in RCM simulations and, in a smaller number of cases, is reversed with cold and wet biases. This spatial correspondence is not visible in the ALADIN 5.3 simulation.

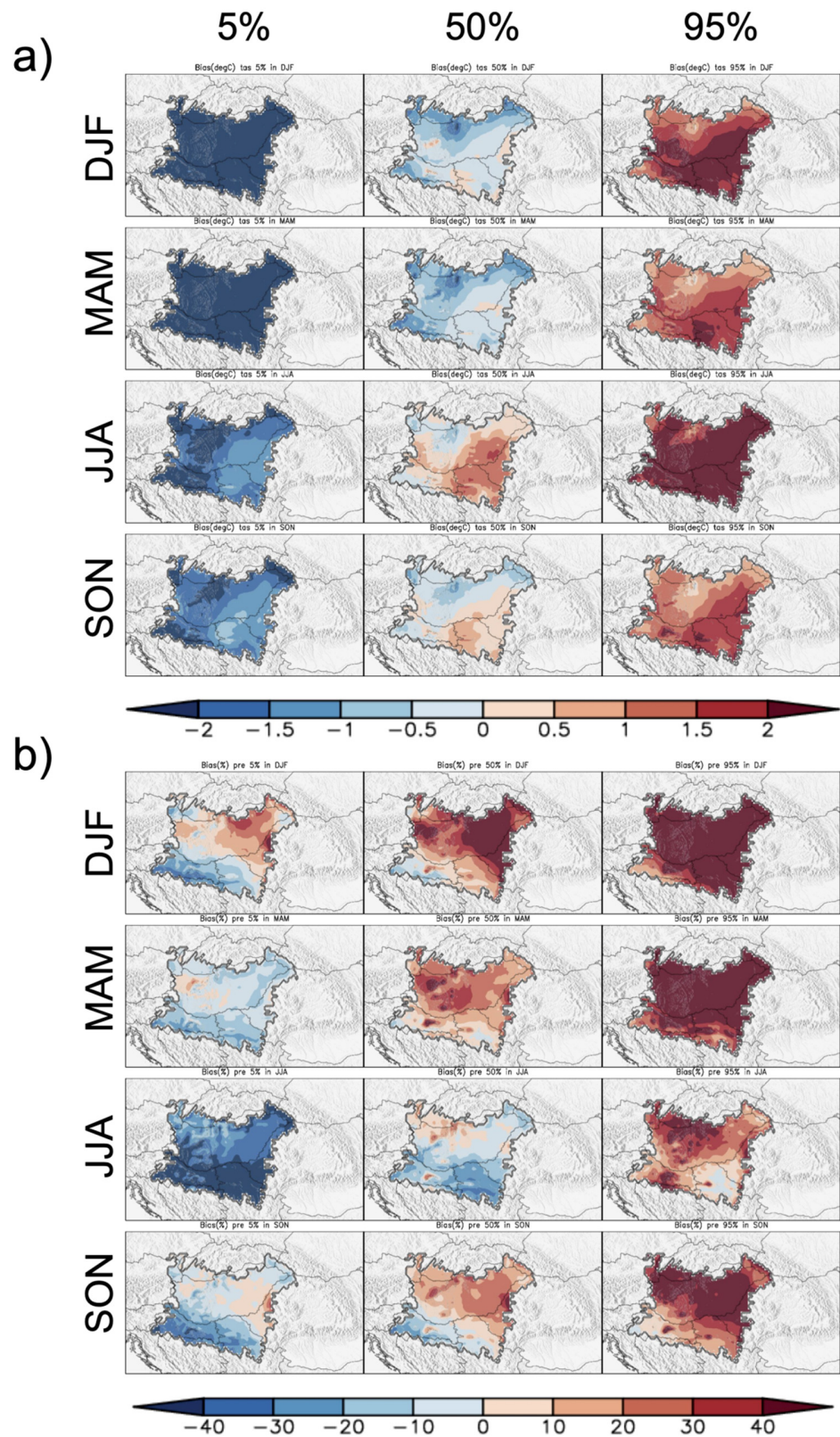


**Figure 3.** Distribution of (a) mean temperature biases (1971–2000) and (b) mean precipitation biases (1971–2000) for the winter season (DJF), spring season (MAM), summer season (JJA), and autumn season (SON). First row, left: 5th percentile of the mean RCM temperature bias among the 30 RCM simulations. Middle: median of the mean RCM temperature bias distribution. Right: 95th percentile of the mean RCM temperature bias distribution.

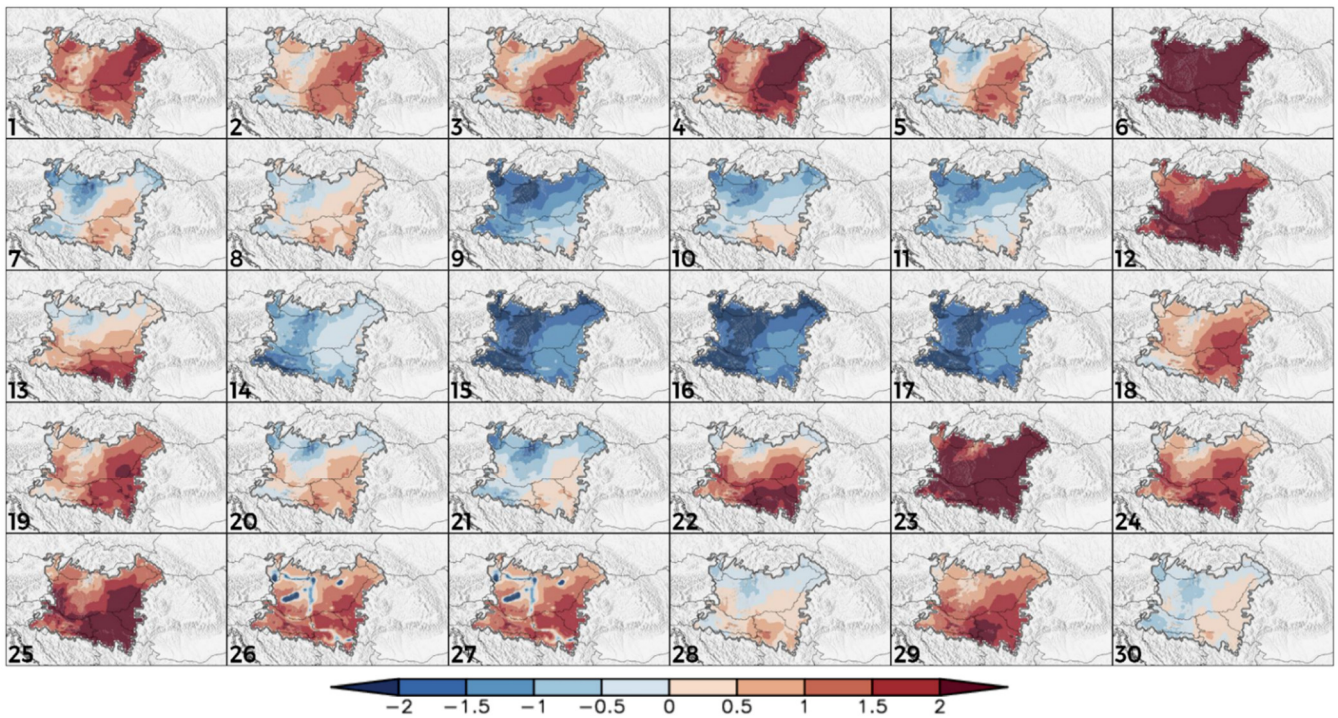


**Figure 4.** Mean (1971–2000) summer GCM–RCM bias of the mean temperature field compared with the E-OBS gridded dataset. Units are °C. The integration numbers follow the list from Table 1.

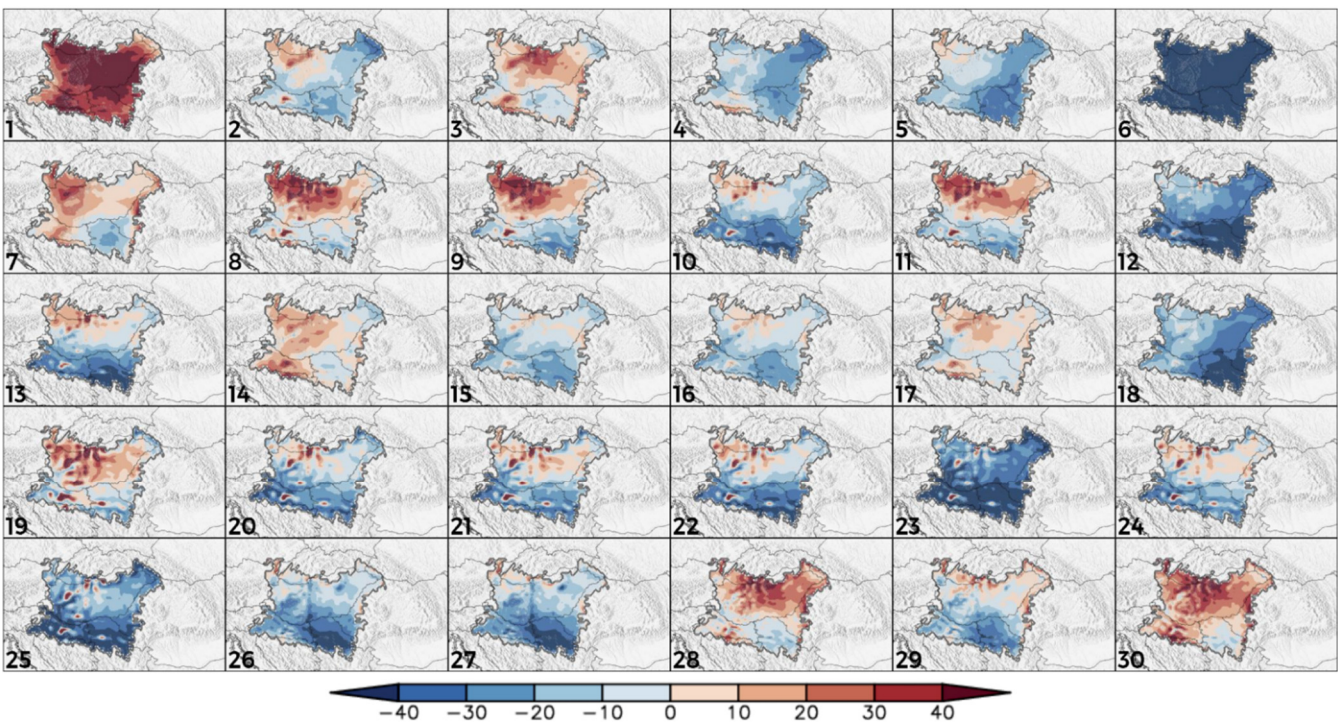


**Figure 5.** Mean (1971–2000) summer GCM–RCM bias of the mean precipitation field compared with the E-OBS gridded dataset. Biases are expressed as % of observations. The integration numbers follow the list from Table 1.

The same RCM is driven by different GCMs to examine the prevailing signal of positive or negative errors (with respect to representing mean temperature) of the corresponding driving models since GCM predominantly determines mean temperature bias [38]. In Figures 4 and 5, strong cold biases are found at a qualitative level, in summer, for the

majority of RCMs downscalings in the EC-EARTH realizations (simulations denoted with numbers 9, 10, 11, 15, 16, 17, and 21), while HadGEM2-ES downscalings with different RCMs (simulations denoted with numbers 6, 12, 18, and 23) have the most pronounced warm and dry biases, which are straightforward in the sense that the overall biases presented in Figures 6 and 7 are not a result of error cancellation. In Figure 4, most RCMs driven with GCMs, such as CNRM-CM5 (simulations denoted with numbers 1, 2, 3, 4, and 19) and NCC-NorESM1-M (simulations denoted with numbers 13, 25, and 29), showed positive temperature bias; however, this warm bias was less pronounced than the warm bias present in HadGEM2-ES downscaling with different RCMs.

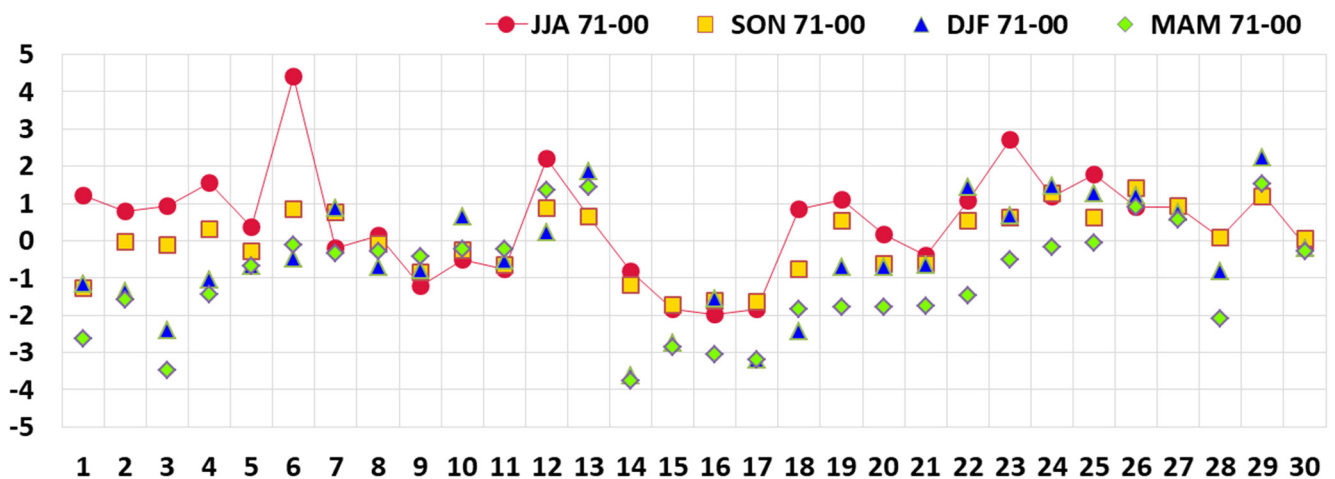


**Figure 6.** Mean (1971–2000) GCM–RCM seasonal bias of the mean temperature field averaged over the Pannonian Basin and compared with the E-OBS gridded dataset. The red line denotes overall bias during the summer. Units are in °C. The integration numbers follow the list from Table 1.

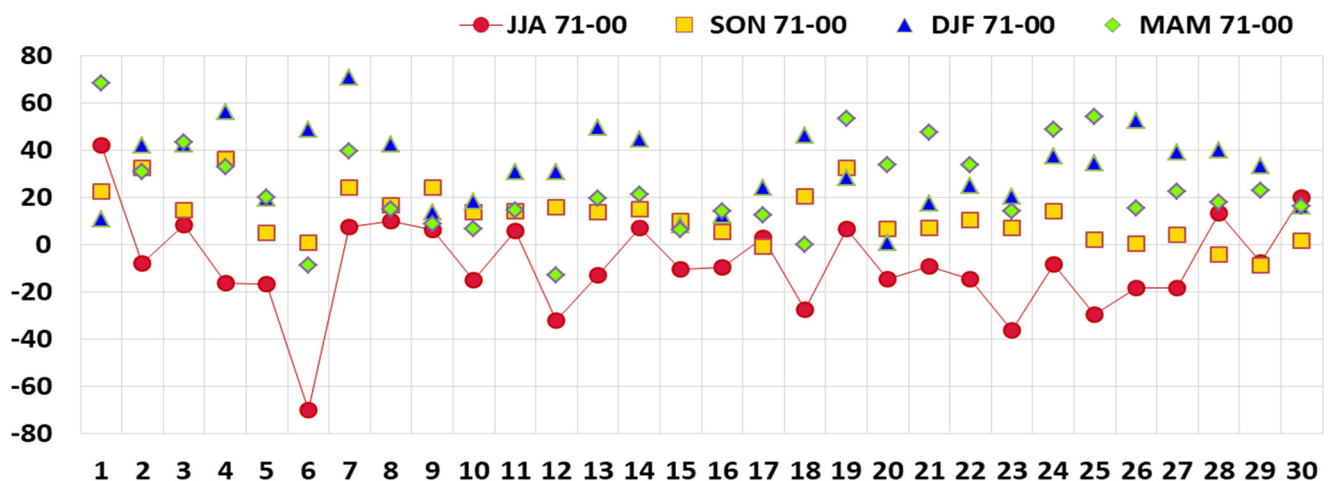


**Figure 7.** Mean (1971–2000) GCM–RCM seasonal bias of the precipitation field averaged over the Pannonian Basin and compared with the E-OBS gridded dataset. The red line denotes overall bias during summer. Biases are expressed as % of observations. The integration numbers follow the list from Table 1.

In support of the abovementioned fact, RCM HIRHAM 5 tends to underestimate summer temperature when forced by GCM EC-EARTH (denoted with numbers 9, 10, and 11), except for simulations denoted with numbers 8, 12, and 13 when driven with GCM CNRM-CM5 (warm bias). RCM RACMO 2.2E (simulations denoted with numbers 14, 15, 16, 17) maintains a strong negative temperature bias during the summer, except in the case when RACMO 2.2E is driven by GCM HadGEM2-ES (simulation denoted with

number 18) since GCM HadGEM2-ES contributes as a warm bias. RCMs ALADIN 5.3 (denoted with number 1) and ALADIN 6.3 (denoted with number 2) were driven by the same GCM with features to overestimate the mean temperature, but ALADIN 5.3 (older version) had a greater positive temperature bias than ALADIN 6.3. Additionally, RCA 4 had a positive mean summer bias of temperature (denoted with numbers 19, 20, 22, 23, 24, and 25), excluding simulation when forced by GCM EC-EARTH (denoted with number 21), which showed cold temperature bias. RCM REMO 2009 (denoted with numbers 26 and 27) maintained a positive summer temperature bias. On the other hand, RCM REMO 2015 had the smallest temperature bias (simulations denoted with numbers 28 and 30), except in the case when it was driven by GCM NCC-NorESM1-M (marked with number 29) because of its positive warm bias contribution. Comparing the results among different RCMs forced by the same GCM when Figures 4 and 6 are concerned, we concluded that RCM CCLM 4.8.17 forced by GCM HadGEM2-ES (denoted with number 6) had the greatest warm bias.

As mentioned, it is difficult to isolate the GCM and RCM contributions from the overall bias for precipitation due to the main drivers of precipitation, such as large-scale drivers and physical parameterizations, but some main and striking conclusions could be made. Figure 5 shows that the previously specified downscaling of the HadGEM2-ES and NCC-NorESM1-M GCMs with different RCMs that overestimate temperature underestimates precipitation. In contrast, RCMs driven with GCM EC-EARTH tend to overestimate precipitation. RCM ALADIN 5.3 has an issue with representing precipitation due to its overestimation, although ALADIN 5.3 also overestimates the mean temperature. However, spatial correspondence between temperature and precipitation bias is observed in RCM ALADIN 6.3, which is driven with the same GCM as ALADIN 5.3. Additionally, RCM CCLM 4.8.17 tends to underestimate precipitation.

These results obtained from Figures 4 and 5 correspond with the results from Reference [38] for the Eastern Europe region where GCM and RCM contributing biases are examined, except that in the Pannonian Basin, temperature bias was even more emphasized for certain GCM–RCM combinations.

Note that the E-OBS reference dataset errors are larger in the summer season for the precipitation field since summer precipitation is mainly convective rather than frontal [38,44]. Hence, verification of the precipitation field with respect to E-OBS has more uncertainty than temperature validations. In addition, as observed in Reference [38], RCMs tend to overestimate precipitation in summer more than in winter due to the E-OBS deficiency in the present observed precipitation field. Hence, we assume that summer precipitation underestimation over the Pannonian Basin is even more pronounced because E-OBS underestimates summer precipitation.

The different parameterizations used in the analyzed RCM simulations or transportable error from GCMs used for downscaling are directly responsible for the broad range of examined GCM–RCM seasonal biases, as we can see in Figures 6 and 7. Temperature and precipitation biases do not remain constant during seasons for a particular GCM–RCM combination, so Figures 6 and 7 indicate a strong time dependence. However, the annual cycle is seen in Figure 6, where most RCMs overestimate summer temperature. According to our findings, in Figures 6 and 7, where spatially averaged overall bias is presented, 17 RCMs overestimate temperature, 8 RCMs underestimate temperature, and 5 RCMs estimate temperature around the E-OBS gridded dataset during the summer season. Most RCMs that overestimate temperature, on the other hand, underestimate precipitation during the summer season. The summer temperature bias ranged from  $-1.9$  to  $+4.4$  °C, while the summer precipitation bias ranged from  $+42\%$  to  $-70\%$ .

Note that in some cases, the near-zero overall mean temperature biases (5 RCMs) presented in Figures 6 and 7 are a result of error cancelations, as seen in Figures 4 and 5. For instance, CCLM4-8-17 driven by MPI-ESM-LR (listed as number 7), HIRHAM 5 driven by CNRM-CM5 (listed as number 8), RCA4 driven by EC-EARTH (listed as number 20), REMO 2015 driven by IPSL-CM5A-LR (listed as number 28) and NOAA-GFDL-GFDL-

ESM2G (listed as number 30) approximately did not show overall summer temperature bias in Figure 6, but we can see the bias in Figure 4.

To examine the “summer drying” issue over the Pannonian Basin in more detail, additional assessments are carried out over a selected subregion in the Carpathian region (Pannonian Basin). In this study, the main goal was to statistically examine the ability of RCMs to represent temperature and precipitation fields in the summer season. The other three seasons are displayed for comparison only.

Three statistics, such as centered RMSE along with the standard deviations and the spatial correlations of RCM simulations of four meteorological variables (tas, tasmax, tasmin, and pre), were assessed against the E-OBS dataset over the Pannonian Basin for the 1971–2000 period in Figures 8–11. Statistics are calculated over all 2205 grid cells of the observed field and from the thirty GCM–RCM simulations, except for tasmax and tasmin, where twenty-nine simulations were available and evaluated. The Taylor diagrams enable us to graphically indicate the individual RCM that is the most realistic compared with the E-OBS dataset. In Figures 8–11, where Taylor diagrams are presented, there is a table that displays a list of evaluated GCM–RCM simulations. In the table, simulations are divided into four parts by an underscore. The first section represents the name of the RCM driven by the GCM determined in the second section, the third section shows the identified realization of the same GCM driver, and the fourth section shows the RCM version.

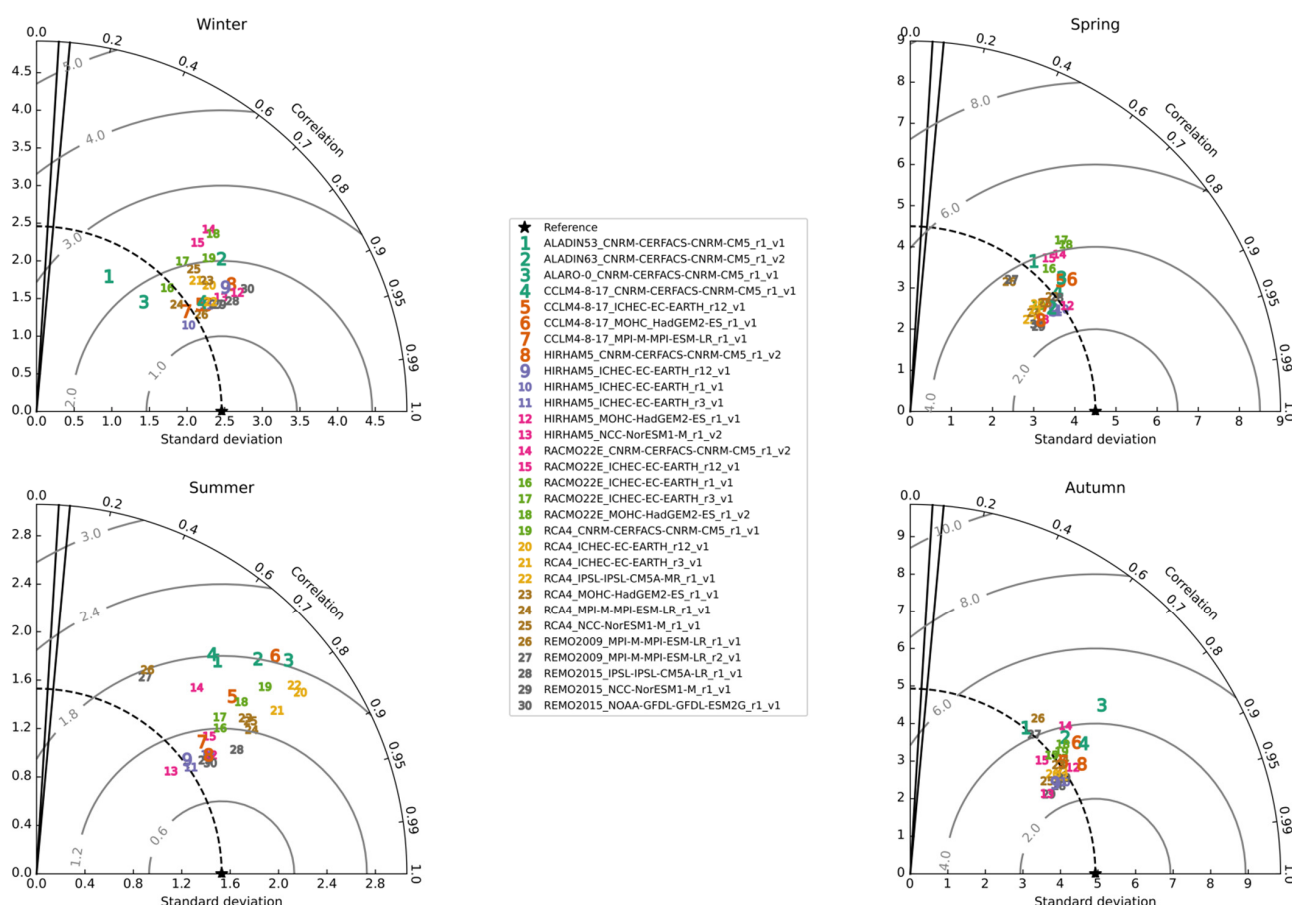


**Figure 8.** Taylor diagrams of seasonal (1971–2000) mean near-surface air temperature showing standard deviation (°C), centered RMSE (°C), and spatial correlation for each EURO-CORDEX GCM–RCM simulation versus E-OBS observations across the Pannonian Basin. The four panels refer to the four seasons defined as winter (DJF), spring (MAM), summer (JJA), and autumn (SON). The observed field is labeled with a star symbol. The dotted line depicts the contour of the reference standard deviation (the observed field). The RMSE contours are grayed out. The 95th and 99th significance levels are represented by the correlation rays on the left and right, respectively.

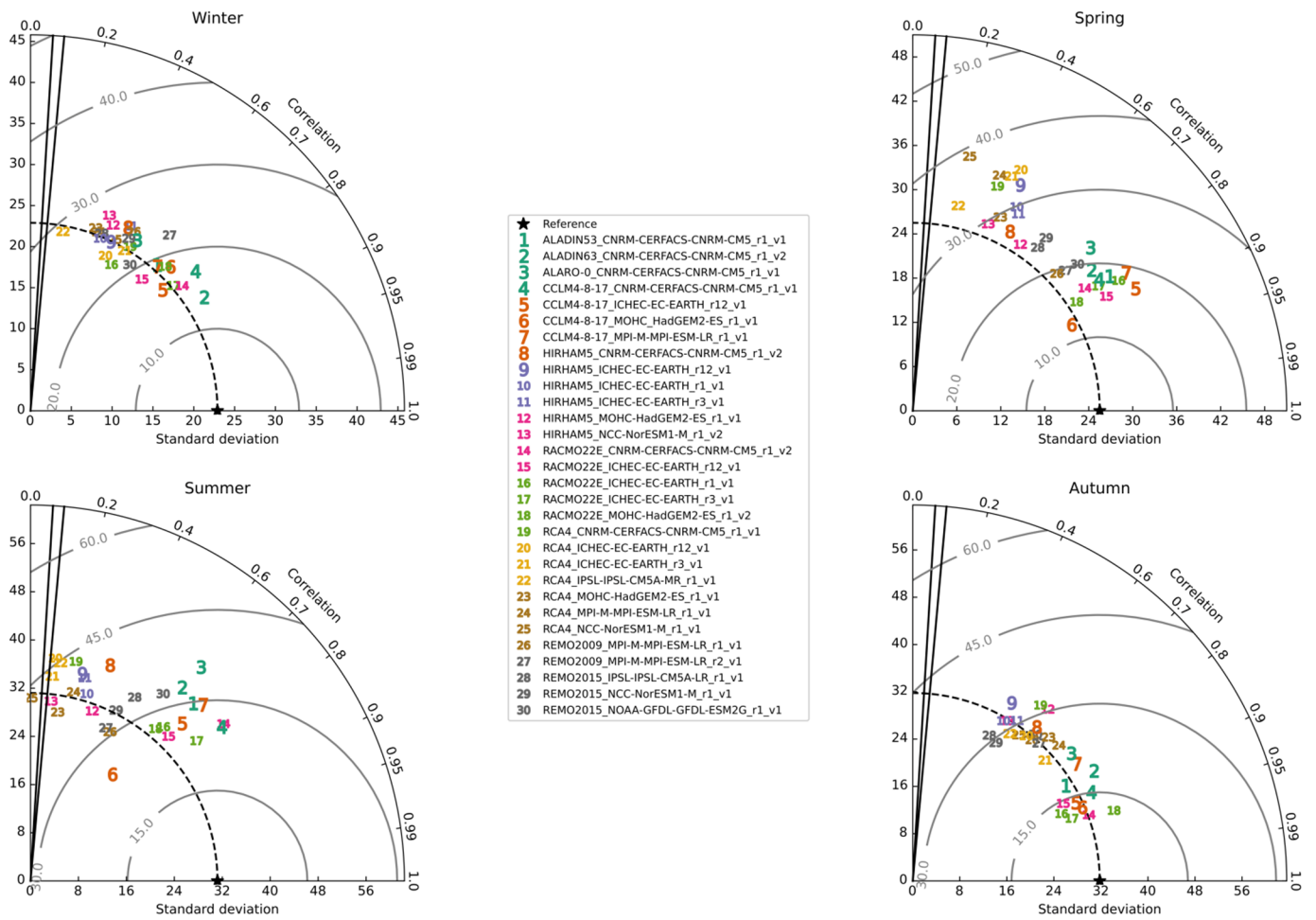


**Figure 9.** Taylor diagrams of seasonal (1971–2000) precipitation showing standard deviation (mm/season), centered RMSE (mm/season), and spatial correlation for each EURO-CORDEX GCM–RCM simulation versus E-OBS observations across the Pannonian Basin. The four panels refer to the four seasons defined as winter (DJF), spring (MAM), summer (JJA), and autumn (SON). The observed field is labeled with a star symbol. The dotted line depicts the contour of the reference standard deviation (the observed field). The RMSE contours are grayed out. The 95th and 99th significance levels are represented by the correlation rays on the left and right, respectively.

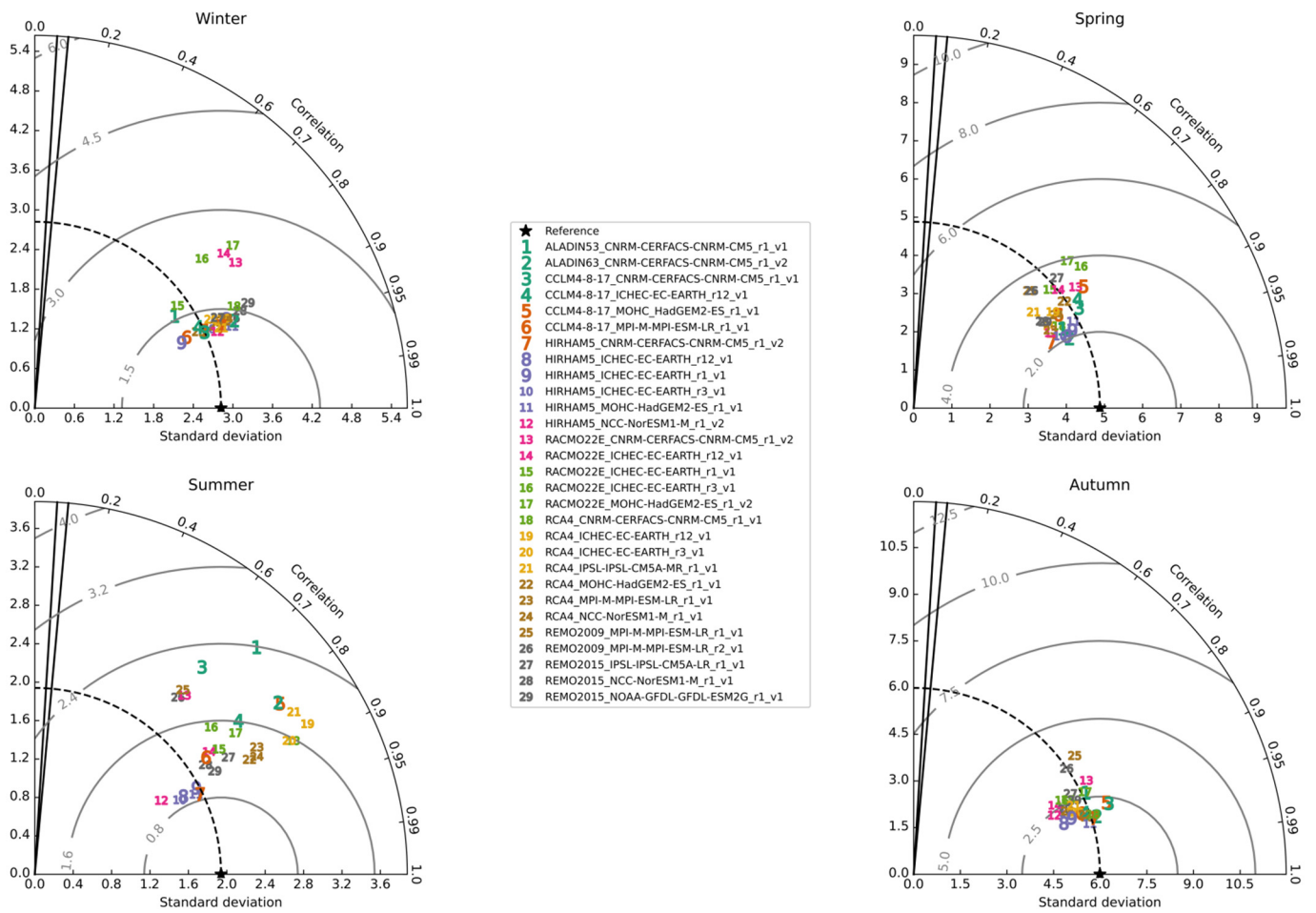


**Figure 10.** Taylor diagrams of seasonal (1971–2000) maximum temperature showing standard deviation ( $^{\circ}\text{C}$ ), centered RMSE ( $^{\circ}\text{C}$ ), and spatial correlation for each EURO-CORDEX GCM–RCM simulation versus E-OBS observations across the Pannonian Basin. The four panels refer to the four seasons defined as winter (DJF), spring (MAM), summer (JJA), and autumn (SON). The observed field is labeled with a star symbol. The dotted line depicts the contour of the reference standard deviation (the observed field). The RMSE contours are grayed out. The 95th and 99th significance levels are represented by the correlation rays on the left and right, respectively.



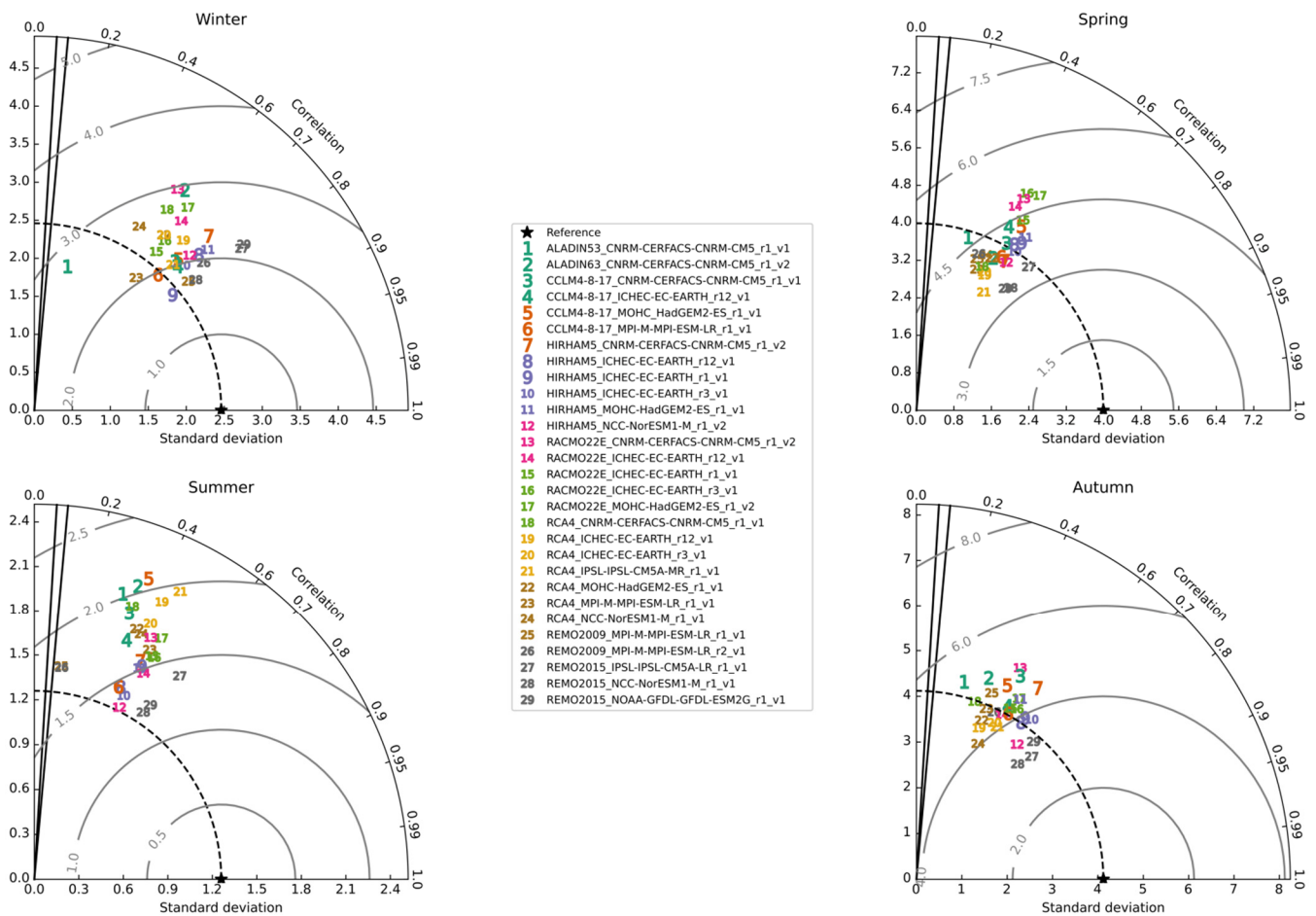


**Figure 11.** Taylor diagrams of seasonal (1971–2000) minimum temperature showing standard deviation ( $^{\circ}\text{C}$ ), centered RMSE ( $^{\circ}\text{C}$ ), and spatial correlation for each EURO-CORDEX GCM–RCM simulation versus E-OBS observations across the Pannonian Basin. The four panels refer to the four seasons defined as winter (DJF), spring (MAM), summer (JJA), and autumn (SON). The observed field is labeled with a star symbol. The dotted line depicts the contour of the reference standard deviation (the observed field). The RMSE contours are grayed out. The 95th and 99th significance levels are represented by the correlation rays on the left and right, respectively.

From Figures 8–11, we notice that for the summer season, the presented scores show the highest spatial variability in comparison to the other three seasons for all examined variables (tas, tasmax, tasmin, and pre), which represent EURO-CORDEX model uncertainty in simulating meteorological fields, as well as disagreement in standard deviation compared with the observed field. This main feature is present to the greatest extent in models’ performance to represent tasmax during summer. If we consider temperature variables (tas, tasmax, and tasmin), the spatial correlation coefficients are the lowest in the model performance to simulate tasmin fields in all seasons (especially in summer). According to [38], this finding could indicate that RCM biases mainly contribute to the overall bias in this case due to deficiency in local physical parameterizations. The lowest spatial correlation coefficients among all four examined fields (tas, tasmax, tasmin, and pre) are noticeable in precipitation fields. On the other hand, the spatial correlation coefficients are the highest in the model performance to simulate tasmax fields. The models overestimate spatial variability in summer (standard deviations of most model fields are constantly high in comparison to the observed field, especially for tas and tasmin), indicating that the models produce wider distributions. Moreover, different realizations of the same GCM driver used to estimate the impact of simulated natural variability on climate change responses do not show significantly different Taylor statistics for the same GCM.

According to Figure 8, grid cell correlations for the mean temperature field are also relatively lower in summer than in the other three seasons, and the spread of correlations ranges between 0.48 and 0.85. Summer correlation coefficients are high in general (most RCMs have correlation coefficients between 0.71 and 0.85). Furthermore, during the summer, in contrast with observations, RCM REMO 2009, with a slightly overestimated standard deviation, had the lowest performance in terms of the spatial correlation coefficient (approximately 0.48) and centered RMSE. In agreement with Figures 4 and 6, REMO 2009 had a slightly wider shifted temperature distribution toward higher values addressed as large positive bias and the largest standard deviation of the model error (centered RMSE), which indicates model inaccuracy. Notably, HIRHAM 5 and REMO 2015 are among the best-performing RCMs (correlation coefficients are high at  $>0.8$ ), especially during the summer, conforming to the Taylor diagram in Figure 8. However, this result does not mean that a temperature bias does not exist in these simulations, as shown in Figure 4. In addition, RCM RCA 4 driven by different GCMs had high spatial correlation coefficients despite the overestimated standard deviations compared with the E-OBS dataset and high centered RMSE during summer. RCM RCA4 showed this common pattern in all three Taylor diagrams where temperature statistics are presented (tas, tasmax, and tasmin).

The same conclusions were observed in the Taylor diagrams for 1951–1980 (see Supplementary Materials Figure S1) and 1961–1990 (see Supplementary Materials Figure S2). RCM RCA 4 did not have available mean temperature data for these periods, so this model is not shown in the Supplementary Materials.

RCM simulations for precipitation (Figure 9), in comparison to temperatures (Figure 8, Figure 10, and Figure 11), indicate lower compliance with observed fields ( $<0.8$  in all cases). Spatial precipitation correlation values for GCM–RCM combinations are much lower than those for temperatures (tas, tasmin, and tasmax) and in some cases are not statistically significant (RCA4 driven by NCC-NorESM1-M numbered 25 in Figure 9). The spread of spatial correlations ranges between close to 0 and 0.78. During winter and autumn, the best compliance with the observed field was observed when all three statistics presented in the Taylor diagram were considered. This finding is in accordance with previous research that suggests that climate models simulate stratiform synoptic-scale precipitation better than local convective precipitation [55].

According to the Taylor diagram in Figure 9, RCMs such as RACMO 2.2E and CCLM 4.8.17 showed the best performance in representing the precipitation field with spatial correlation coefficients higher than 0.6, although in Figure 5, these RCMs had a nonzero bias. These RCMs have a mostly wider precipitation distribution toward lower values, which is addressed as a large negative bias and the lowest standard deviation of model error (centered RMSE). The RCMs with the lowest score were RCA 4 with spatial correlation coefficients lower than 0.2. These findings are consistent with previous work for the Carpathian region [49]. Additionally, even though RCMs REMO 2015 and HIRHAM 5 showed the best performance according to the temperature verification, these RCMs realized lesser performances with spatial correlation coefficients lower than 0.6 with respect to the evaluation precipitation field. REMO 2015 is slightly better than HIRHAM 5 according to the three precipitation statistics displayed in Figure 9.

The same conclusions were observed in Taylor diagrams for periods of 1951–1980 (see Supplementary Materials Figure S3) and 1961–1990 (see Supplementary Materials Figure S4). RCM RCA 4 did not have available precipitation data for these periods, so this model is not shown in the Supplementary Materials.

According to Figure 10, similar RCM performances are observed in representing tasmax as those representing tas during the summer. The main difference is that RCMs showed the highest spatial variability during summer in comparison with the other three seasons in representing the maximum temperature field. This result is because HIRHAM 5 underestimates the standard deviation compared with the observed field, while other RCMs overestimate the standard deviations. During summer, the spread of correlations is between 0.62 and 0.90, reflecting the highest correlations among the other three variables

(tas, tasmin, and pre). The correlation coefficients in summer are generally high (most RCMs have correlation coefficients between 0.76 and 0.89). The best-performing RCMs during summer are REMO 2015 and HIRHAM 5, with spatial correlation coefficients higher than 0.85 and with slightly more enhanced performances to represent tasmax than representing tas. Generally, RCMs have better statistical scores in representing tasmax than tas in summer. On the other hand, REMO 2009 has poorer scores, as was the case with tas. In line with Figure 10, the lesser performances in summer are from RCMs ALADIN 5.3 and CCLM 4.8.17 driven by CNRM-CM5. RCM ALADIN 6.3 realized a better performance with respect to the Taylor statistics than RCM ALADIN 5.3.

Figure 11 shows that the RCM performances for tasmin fields in the summer season are worse than the performances for tas and tasmax with regard to all three statistics, especially concerning a spatial correlation coefficient. During summer, the spread of correlations is between 0.12 and 0.58. RCM REMO 2009 had the lowest scores (the highest RMSE values) in representing tasmin due to the largest centered RMSE and the lowest spatial correlation coefficient (0.12). RCMs REMO 2015 are among the top models in representing tasmin, with a spatial correlation coefficient of approximately 0.5.

Finally, as an additional metric of the model performance, we examined the temperature trend over the period of 1970–2005. The results from Table 2 show that RCMs had a positive trend in the observed field for the last 36 years (only RCM HIRHAM 5 driven by GCM NCC-NorESM1-M did not show either positive or negative trends). The RCMs that showed the smallest departure from the observed temperature trend were ALADIN 5.3, CCLM 4.8.17 driven by EC-EARTH r12 and HadGEM2-ES, HIRHAM 5 driven by HadGEM2-ES, RACMO 2.2E driven by EC-EARTH r12, RCA 4 driven by MPI-ESM-LR, and REMO 2015 driven by NCC-NorESM1-M and NOAA-GFDL-GFDL-ESM2G. The temperature trends and temperature summer bias do not seem to be connected, which means that warm/cold summer temperature bias does not indicate overestimated/underestimated temperature trends compared with the E-OBS dataset and reverse.

**Table 2.** Temperature trends averaged over the Pannonian Basin of the EURO-CORDEX RCMs and E-OBS during the 1970–2005 period.

GCM-RCMs	Trend in °C/Decade	GCM-RCMs	Trend in °C/Decade
1. ALADIN53_CNRM-CERFACS-CNRM-CM5_r1_v1	0.24	16. RACMO22E_ICHEC-EC-EARTH_r1_v1	0.54
2. ALADIN63_CNRM-CERFACS-CNRM-CM5_r1_v2	0.54	17. RACMO22E_ICHEC-EC-EARTH_r3_v1	0.69
3. ALARO-0_CNRM-CERFACS-CNRM-CM5_r1_v1	0.20	18. RACMO22E_MOHC-HadGEM2-ES_r1_v2	0.43
4. CCLM4-8-17_CNRM-CERFACS-CNRM-CM5_r1_v1	0.06	19. RCA4_CNRM-CERFACS-CNRM-CM5_r1_v1	0.14
5. CCLM4-8-17_ICHEC-EC-EARTH_r12_v1	0.23	20. RCA4_ICHEC-EC-EARTH_r12_v1	0.21
6. CCLM4-8-17_MOHC-HadGEM2-ES_r1_v1	0.24	21. RCA4_ICHEC-EC-EARTH_r3_v1	0.48
7. CCLM4-8-17_MPI-M-MPI-ESM-LR_r1_v1	0.18	22. RCA4_IPSL-IPSL-CM5A-MR_r1_v1	0.37
8. HIRHAM5_CNRM-CERFACS-CNRM-CM5_r1_v2	0.48	23. RCA4_MOHC-HadGEM2-ES_r1_v1	0.31
9. HIRHAM5_ICHEC-EC-EARTH_r12_v1	0.16	24. RCA4_MPI-M-MPI-ESM-LR_r1_v1	0.30
10. HIRHAM5_ICHEC-EC-EARTH_r1_v1	0.31	25. RCA4_NCC-NorESM1-M_r1_v1	0.17
11. HIRHAM5_ICHEC-EC-EARTH_r3_v1	0.37	26. REMO2009_MPI-M-MPI-ESM-LR_r1_v1	0.06
12. HIRHAM5_MOHC-HadGEM2-ES_r1_v1	0.30	27. REMO2009_MPI-M-MPI-ESM-LR_r2_v1	0.19
13. HIRHAM5_NCC-NorESM1-M_r1_v2	0.00	28. REMO2015_IPSL-IPSL-CM5A-LR_r1_v1	0.16
14. RACMO22E_CNRM-CERFACS-CNRM-CM5_r1_v2	0.41	29. REMO2015_NCC-NorESM1-M_r1_v1	0.27
15. RACMO22E_ICHEC-EC-EARTH_r12_v1	0.23	30. REMO2015_NOAA-GFDL-GFDL-ESM2G_r1_v1	0.30
E-OBS	0.26		

#### 4. Conclusions

RCMs are valuable sources of fine-scale climate information because they are often used as input to assess the impact of possible climate change in the future on certain socioeconomic sectors of society or the environment. The main goal of the present study was to test whether dry and warm biases existed in summer over the Pannonian Basin in thirty RCM simulations of the EURO-CORDEX initiative, as was the case in previously mentioned studies and projects of dynamic downscaling across Southeastern Europe. All verification scores in this paper are evaluated for the domain of the Pannonian Basin and for

temperature and precipitation fields. According to our GCM–RCM evaluation, we conclude that none of the GCM–RCM pairs are improbable. On the other hand, the ensemble has systematic biases, and the simulations have common deviations from observations. Our results confirmed that, in summer, in many different RCM simulations, dry and warm biases were detected across the Pannonian Basin; however, few RCMs showed cold and wet biases. The median of the simulations is hotter and drier than that observed in the Pannonian Basin during the summer, with the widest RCM simulation distribution. Furthermore, we observed that, for all examined variables (tas, tasmax, tasmin, and pre), verification scores in the summer season displayed the highest spatial variability in comparison to the other three seasons, which represents EURO-CORDEX model uncertainty in simulating meteorological fields.

Generally, determining the best or worst GCM–RCM pair is futile because the skills are highly dependent on the area and examined meteorological field. However, in this study, we limited ourselves to the area of the Pannonian Basin. The RCM that stands out with good scores in simulating temperature fields is REMO 2015; and, on the other hand, good performance in representing the precipitation field showed RACMO 2.2E and CCLM 4.8.17. In conclusion, RCMs with good performances in representing temperatures do not necessarily perform well in representing precipitation, and vice versa. In general, and considering only temperatures, RCMs have the best statistical scores representing maximum temperature and the worst statistical scores in representing minimum temperature. However, the same RCM driven by certain GCMs showed similar tendencies in representing all three temperature fields (tas, tasmax, and tasmin). On the other hand, the lowest spatial correlation coefficients among all four examined fields (tas, tasmax, tasmin, and pre) were present in precipitation fields. However, most RCMs that overestimate temperature also underestimate precipitation.

Hence, one of the possible reason for the observed summer drying problem may be in representation interaction and feedback between soil moisture (land) and atmosphere and, for instance, in the false representation of soil type [28]. As mentioned before, soil type defines parameters that have a major impact on soil moisture conditions and surface fluxes. Soil moisture is an essential feature of the land–atmosphere interaction that affects the conditions on the surface, such as radiation and humidity [28]. Therefore, our next goal in further researches is to examine the soil moisture–atmosphere interactions in RCM in the Pannonian Basin (such as investigating annual cycle of soil moisture for soil layers after changing the soil type, comparing RCM soil moisture data with observed data, etc.) in order to reduce to some extent warm and dry bias. It is important to note that according to a former study [56], it is found that one of the primary sources and trigger for dry and warm bias in the summer season is precipitation deficit regarding the fact that local and small-scale convection systems are not captured well in RCMs. Precipitation deficit thereafter is followed by complex land–atmosphere interactions that cause the positive bias in temperature fields. Initial intention in this paper was to check if high-resolution runs (that were not available in the past) helped in terms of negative precipitation and positive temperature bias in the region, in the first place by better representation of convective precipitation during the summer. Our hypothesis was that higher resolution will lead to more localized and higher convective precipitation (a common feature of the models) that can reduce some of the biases. To our surprise, some of the models, even though they have run in high-resolution mode, still produce similar errors, as low-resolution ones (comparing with previously published research on this topic). We found this very interesting as proof that higher resolution is not simply a solution to some ‘old well-known biases’. Consequently, to better understand the sources and reasons for the summer drying problem to improve the ability of RCMs to represent the past climate in the Pannonian Basin, further research is needed. The results from the driving GCMs should also be verified to determine the effect of various lateral boundary conditions on the results from RCM simulations and to examine the added value of downscaling more thoroughly in RCMs.

**Supplementary Materials:** The following are available online at <https://www.mdpi.com/article/10.3390/atmos12060714/s1>.

**Author Contributions:** Conceptualization, V.D. and I.L.; Data curation, I.L. and M.T.; Formal analysis, I.L. and M.T.; Investigation, I.L.; Methodology, I.L.; Visualization, I.L. and M.T.; Writing—original draft, I.L. All authors have read and agreed to the published version of the manuscript.

**Funding:** This research was funded by the Ministry of Education, Science and Technological Development of the Republic of Serbia, No. 451-03-9/2021-14/200162.

**Institutional Review Board Statement:** Not applicable.

**Informed Consent Statement:** Not applicable.

**Data Availability Statement:** Data is contained within the article and Supplementary Material.

**Acknowledgments:** The authors would like to thank the EURO-CORDEX framework for making multi-model ensemble data accessible; the ECA&D project, which provided us with free gridded observation E-OBS dataset; and the Max Planck Institute for Meteorology, which enabled free software CDO (The Climate Data Operators) for the processing of climate data. The authors are also grateful to the anonymous reviewers for their thorough revision of the manuscript, which significantly improved the paper's quality.

**Conflicts of Interest:** The authors declare no conflict of interest.

## References

1. Arritt, R.W.; Rummukainen, M. Challenges in regional-scale climate modeling. *Bull. Am. Meteorol. Soc.* **2011**, *92*, 365–368. [[CrossRef](#)]
2. Giorgi, F. Thirty years of regional climate modeling: Where are we and where are we going next? *J. Geophys. Res. Atmos.* **2019**, *124*, 5696–5723. [[CrossRef](#)]
3. Rawlins, M.A.; Bradley, R.S.; Diaz, H.F. Assessment of regional climate model simulation estimates over the northeast United States. *J. Geophys. Res. Atmos.* **2012**, *117*, D23112. [[CrossRef](#)]
4. Giorgi, F. Regional climate modeling: Status and perspectives. *J. Phys. IV France* **2006**, *139*, 101–118. [[CrossRef](#)]
5. Heikkilä, U.; Sandvik, A.; Sorteberg, A. Dynamical downscaling of ERA-40 in complex terrain using the WRF regional climate models. *Clim. Dyn.* **2011**, *37*, 1551–1564. [[CrossRef](#)]
6. Giorgi, F.; Hurrell, J.W.; Marinucci, M.R.; Beniston, M. Elevation dependency of the surface climate change signal: A model study. *J. Clim.* **1997**, *10*, 288–296. [[CrossRef](#)]
7. Torma, C.; Giorgi, F.; Coppola, E. Added value of regional climate modeling over areas characterized by complex terrain—Precipitation over the Alps. *J. Geophys. Res. Atmos.* **2015**, *120*, 3957–3972. [[CrossRef](#)]
8. Prein, A.F.; Gobiet, A.; Suklitsch, M.; Truhetz, H.; Awan, N.K.; Keuler, K.; Georgievski, G. Added value of convection permitting seasonal simulations. *Clim. Dyn.* **2013**, *41*, 2655–2677. [[CrossRef](#)]
9. Giorgi, F.; Torma, C.; Coppola, E.; Ban, N.; Schär, C.; Somot, S. Enhanced summer convective rainfall at Alpine high elevations in response to climate warming. *Nat. Geosci.* **2016**, *9*, 584–589. [[CrossRef](#)]
10. Coppola, E.; Sobolowski, S.; Pichelli, E.; Raffaele, F.; Ahrens, B.; Anders, I.; Ban, N.; Bastin, S.; Belda, M.; Belusic, D.; et al. A first-of-its-kind multi-model convection permitting ensemble for investigating convective phenomena over Europe and the Mediterranean. *Clim. Dyn.* **2020**, *55*, 3–34. [[CrossRef](#)]
11. Di Luca, A.; Argüeso, D.; Evans, J.P.; de Elía, R.; Laprise, R. Quantifying the overall added value of dynamical downscaling and the contribution from different spatial scales. *J. Geophys. Res. Atmos.* **2016**, *121*, 1575–1590. [[CrossRef](#)]
12. Di Luca, A.; de Elía, R.; Laprise, R. Challenges in the quest for added value of regional climate dynamical downscaling. *Curr. Clim. Chang. Rep.* **2015**, *1*, 10–21. [[CrossRef](#)]
13. Diaconescu, E.P.; Laprise, R. Can added value be expected in RCM-simulated large scales? *Clim. Dyn.* **2013**, *41*, 1769–1800. [[CrossRef](#)]
14. Veljovic, K.; Rajkovic, B.; Fennessy, M.J.; Altshuler, E.L.; Mesinger, F. Regional climate modeling: Should one attempt improving on the large scales? Lateral boundary condition scheme: Any impact? *Meteorol. Z.* **2010**, *19*, 237–246. [[CrossRef](#)]
15. Hawkins, E.; Sutton, R. The potential to narrow uncertainty in regional climate predictions. *Bull. Am. Meteorol. Soc.* **2009**, *90*, 1095–1108. [[CrossRef](#)]
16. Meehl, G.A.; Boer, G.J.; Covey, C.; Latif, M.; Stouffer, R.J. The coupled model intercomparison project (CMIP). *Bull. Am. Meteorol. Soc.* **2000**, *81*, 313–318. [[CrossRef](#)]
17. Coppola, E.; Nogherotto, R.; Ciarlo', J.M.; Giorgi, F.; van Meijgaard, E.; Kadygrov, N.; Iles, C.; Corre, L.; Sandstad, M.; Somot, S.; et al. Assessment of the European climate projections as simulated by the large EURO-CORDEX regional climate model ensemble. *J. Geophys. Res. Atmos.* **2021**, *126*. [[CrossRef](#)]

18. Jacob, D.; Teichmann, C.; Sobolowski, S.; Katragkou, E.; Anders, I.; Belda, M.; Benestad, R.; Boberg, F.; Buonomo, E.; Cardoso, R.M.; et al. Regional climate downscaling over Europe: Perspectives from the EURO-CORDEX community. *Reg. Environ. Chang.* **2020**, *20*, 1–20. [[CrossRef](#)]
19. Jacob, D.; Petersen, J.; Eggert, B.; Alias, A.; Christensen, O.B.; Bouwer, L.M.; Braun, A.; Colette, A.; Déqué, M.; Georgievski, G.; et al. EURO-CORDEX: New high-resolution climate change projections for European impact research. *Reg. Environ. Chang.* **2014**, *14*, 563–578. [[CrossRef](#)]
20. Hagemann, S.; Botzet, M.; Machenhauer, B. The summer drying problem over southeastern Europe: Sensitivity of the limited area model HIRHAM4 to improvements in physical parameterization and resolution. *Phys. Chem. Earth Part B Hydrol. Ocean. Atmos.* **2001**, *26*, 391–396. [[CrossRef](#)]
21. Machenhauer, B.; Windelband, M.; Botzet, M.; Hesselbjerg-Christensen, J.; Déqué, M.; Jones, R.G.; Ruti, P.M.; Visconti, G. *Validation and Analysis of Regional Present-Day Climate and Climate Change Simulations over Europe, Report 275*; Report/Max-Planck-Institute for Meteorology: Hamburg, Germany, 1998. Available online: <http://hdl.handle.net/21.11116/0000-0005-803D-6> (accessed on 30 April 2021).
22. Hagemann, S.; Botzet, M.; Dilmenil, L.; Machenhauer, B. *Derivation of Global GCM Boundary Conditions from 1 Km Land Use Satellite Data, Report 289*; Report/Max-Planck-Institute for Meteorology: Hamburg, Germany, 1999. Available online: <http://hdl.handle.net/21.11116/0000-0000-F816-0> (accessed on 30 April 2021).
23. Hagemann, S.; Machenhauer, B.; Jones, R.; Christensen, O.B.; Déqué, M.; Jacob, D.; Vidale, P.L. Evaluation of water and energy budgets in regional climate models applied over Europe. *Clim. Dyn.* **2004**, *23*, 547–567. [[CrossRef](#)]
24. Seneviratne, S.I.; Lüthi, D.; Litschi, M.; Schär, C. Land–atmosphere coupling and climate change in Europe. *Nature* **2006**, *443*, 205–209. [[CrossRef](#)]
25. Seneviratne, S.I.; Corti, T.; Davin, E.L.; Hirschi, M.; Jaeger, E.B.; Lehner, I.; Orlowsky, B.; Teuling, A.J. Investigating soil moisture–climate interactions in a changing climate: A review. *Earth Sci. Rev.* **2010**, *99*, 125–161. [[CrossRef](#)]
26. Denissen, J.M.; Teuling, A.J.; Reichstein, M.; Orth, R. Critical soil moisture derived from satellite observations over Europe. *J. Geophys. Res. Atmos.* **2020**, *125*, 125. [[CrossRef](#)]
27. Koster, R.D.; Dirmeyer, P.A.; Guo, Z.; Bonan, G.; Chan, E.; Cox, P.; Gordon, C.T.; Kanae, S.; Kowalczyk, E.; Lawrence, D.; et al. Regions of strong coupling between soil moisture and precipitation. *Science* **2004**, *305*, 1138–1140. [[CrossRef](#)]
28. Anders, I.; Rockel, B. The influence of prescribed soil type distribution on the representation of present climate in a regional climate model. *Clim. Dyn.* **2009**, *33*, 177–186. [[CrossRef](#)]
29. Szépszó, G. The Adaptation of the REMO Regional Climate Model at the Hungarian Meteorological Service. Available online: <https://citeseerx.ist.psu.edu/viewdoc/download?doi=10.1.1.129.9318&rep=rep1&type=pdf> (accessed on 30 April 2021).
30. Ceglár, A.; Croitoru, A.E.; Cuxart, J.; Djurdjevic, V.; Güttler, I.; Ivančan-Picek, B.; Jug, D.; Lakatos, M.; Weidinger, T. PannEx: The Pannonian Basin Experiment. *Clim. Serv.* **2018**, *11*, 78–85. [[CrossRef](#)]
31. Spinoni, J.; Lakatos, M.; Szentimrey, T.; Bihari, Z.; Szalai, S.; Vogt, J.; Antofie, T. Heat and cold waves trends in the Carpathian Region from 1961 to 2010. *Int. J. Climatol.* **2015**, *35*, 4197–4209. [[CrossRef](#)]
32. Bartholy, J.; Pongrácz, R. Tendencies of extreme climate indices based on daily precipitation in the Carpathian Basin for the 20th century. *Időjárás* **2005**, *109*, 1–20.
33. Vučetić, V.; Feist, O. Heat stress and agriculture in Croatia: Past, present and future. In Proceedings of the GEWEX Workshop on the Climate System of the Pannonian Basin, Osijek, Hrvatska, 9–11 November 2015; p. 1.
34. Lakatos, M.; Bihari, Z.; Szentimrey, T.; Spinoni, J.; Szalai, S. Analyses of temperature extremes in the Carpathian Region in the period 1961–2010. *Időjárás Q. J. Hung. Meteorol. Serv.* **2016**, *120*, 41–51.
35. Kotlarski, S.; Keuler, K.; Christensen, O.B.; Colette, A.; Deque, M.; Gobiet, A.; Goergen, K.; Jacob, D.J.; Lüthi, D.; Van Meijgaard, E.; et al. Regional climate modelling on European scales: A joint standard evaluation of the EURO-CORDEX RCM ensemble. *Geosci. Model Dev.* **2014**, *7*, 1297–1333. [[CrossRef](#)]
36. PannEx White Book A GEWEX Regional Hydroclimate Project (RHP) over the Pannonian Basin. In *WCRP Report 3/2019*; World Climate Research Programme (WCRP): Geneva, Switzerland, 2019; p. 108.
37. Torma, C.Z. Detailed validation of EURO-CORDEX and Med-CORDEX regional climate model ensembles over the Carpathian Region. *Időjárás Q. J. Hung. Meteorol. Serv.* **2019**, *123*, 217–240. [[CrossRef](#)]
38. Vautard, R.; Kadyrov, N.; Iles, C.; Boberg, F.; Buonomo, E.; Bülow, K.; Coppola, E.; Corre, L.; Van Meijgaard, E.; Nogherotto, R.; et al. Evaluation of the large EURO-CORDEX regional climate model ensemble. *J. Geophys. Res. Atmos.* **2020**. [[CrossRef](#)]
39. Christensen, O.B.; Kjellström, E. Partitioning uncertainty components of mean climate and climate change in a large ensemble of European regional climate model projections. *Clim. Dyn.* **2020**, *54*, 4293–4308. [[CrossRef](#)]
40. Foley, A.M. Uncertainty in regional climate modelling: A review. *Prog. Phys. Geogr.* **2010**, *34*, 647–670. [[CrossRef](#)]
41. European Climate Assessment and Datasets. Available online: <https://www.ecad.eu/> (accessed on 28 March 2021).
42. Cornes, R.C.; van der Schrier, G.; van den Besselaar, E.J.; Jones, P.D. An Ensemble Version of the E-OBS Temperature and Precipitation Datasets. *J. Geophys. Res. Atmos.* **2018**, *123*, 9391–9409. [[CrossRef](#)]
43. Klein Tank, A.M.G.K.; Wijngaard, J.B.; Können, G.P.; Böhm, R.; Demarée, G.; Gocheva, A.; Mileta, M.; Pashiardis, S.; Hejkrlik, L.; Kern-Hansen, C.; et al. Daily dataset of 20th-century surface air temperature and precipitation series for the European Climate Assessment. *Int. J. Clim.* **2002**, *22*, 1441–1453. [[CrossRef](#)]

44. Hofstra, N.; Haylock, M.; New, M.; Jones, P.D. Testing E-OBS European high-resolution gridded data set of daily precipitation and surface temperature. *J. Geophys. Res. Atmos.* **2009**, *114*. [[CrossRef](#)]
45. Hofstra, N.; New, M.; McSweeney, C. The influence of interpolation and station network density on the distribution and extreme trends of climate variables in gridded data. *Clim. Dyn.* **2010**, *35*, 841–858. [[CrossRef](#)]
46. Kyselý, J.; Plavcová, E. A critical remark on the applicability of E-OBS European gridded temperature data set for validating control climate simulations. *J. Geophys. Res. Atmos.* **2010**, *115*. [[CrossRef](#)]
47. Min, E.; Hazeleger, W.; van Oldenborgh, G.J.; Sterl, A. Evaluation of trends in high temperature extremes in north-western Europe in regional climate models. *Environ. Res. Lett.* **2013**, *8*, 014011. [[CrossRef](#)]
48. Lenderink, G. Exploring metrics of extreme daily precipitation in a large ensemble of regional climate model simulations. *Clim. Res.* **2010**, *44*, 151–166. [[CrossRef](#)]
49. Kotlarski, S.; Szabó, P.; Herrera, S.; Rätty, O.; Keuler, K.; Soares, P.M.; Cardoso, R.M.; Bosshard, T.; Pagé, C.; Boberg, F.; et al. Observational uncertainty and regional climate model evaluation: A pan-European perspective. *Int. J. Climatol.* **2017**, *39*, 3730–3749. [[CrossRef](#)]
50. Prein, A.F.; Gobiet, A. Impacts of uncertainties in European gridded precipitation observations on regional climate analysis. *Int. J. Climatol.* **2017**, *37*, 305–327. [[CrossRef](#)] [[PubMed](#)]
51. Kendon, E.J.; Jones, R.G.; Kjellström, E.; Murphy, J.M. Using and designing GCM–RCM ensemble regional climate projections. *J. Clim.* **2010**, *23*, 6485–6503. [[CrossRef](#)]
52. Schulzweida, U. *CDO User Guide*; Version 1.9.6; Max Planck Institute for Meteorology: Hamburg, Germany, 2019. [[CrossRef](#)]
53. Taylor, K.E. Summarizing multiple aspects of model performance in a single diagram. *J. Geophys. Res.* **2001**, *106*, 7183–7192. [[CrossRef](#)]
54. Separovic, L.; De Elia, R.; Laprise, R. Reproducible and irreproducible components in ensemble simulations with a regional climate model. *Mon. Weather Rev.* **2008**, *136*, 4942–4961. [[CrossRef](#)]
55. Mearns, L.O.; Giorgi, F.; McDaniel, L.; Shields, C. Analysis of daily variability of precipitation in a nested regional climate model: Comparison with observations and doubled CO<sub>2</sub> results. *Glob. Planet. Chang.* **1995**, *10*, 55–78. [[CrossRef](#)]
56. Lin, Y.; Dong, W.; Zhang, M.; Xie, Y.; Xue, W.; Huang, J.; Luo, Y. Causes of model dry and warm bias over central US and impact on climate projections. *Nat. Commun.* **2017**, *8*, 881. [[CrossRef](#)]